MATHEMATICAL MODELING AND COMPUTING, Vol. 12, No. 1, pp. 57–66 (2025)

Haar wavelet collocation method for solving boundary layer flow and heat transfer over a moving plate in a carbon nanotubes with MHD effect

Haswaniza N. S.[1], Rasedee A. F. N.[2], Bachok N.[1], Wong T. J.[3], Hasan M.[4]

[1]*Department of Mathematics and Statistics, Faculty of Science, University Putra Malaysia, 43400 Serdang, Selangor, Malaysia*
[2]*Faculty of Economics and Muamalat, University Sains Islam Malaysia, Malaysia*
[3]*Department of Basic Sciences and Engineering, Faculty of Agriculture and Food Science, University Putra Malaysia, Bintulu Campus, Nyabau Road, Bintulu, Sarawak, 97008, Malaysia*
[4]*Centre for Foundation Studies in Science of University Putra Malaysia*

(Received 18 October 2024; Revised 4 December 2024; Accepted 9 December 2024)

This study aims to explore the consideration of boundary layer flow and heat transfer over a moving plate with the presence of the magneto-hydrodynamics at the surface in carbon nanotubes. The mathematical model for the boundary layer flow problem is obtained and solved using numerical techniques based on Haar wavelet collocation. The types of nanoparticles used in this research were single-walled carbon nanotubes and multi-walled carbon nanotubes with water and kerosene that were used as base fluid. The partial differential equations are transformed into nonlinearly ordinary differential equations by similarity transformation. Maple software is used to work on these equations. The results were represented in the formation of graphs including velocity and temperature profile, skin friction coefficient and local Nusselt number for different values of magnetic field, CNTs volume friction and moving parameter. The outcomes obtained are that the moving plate gives non-unique solutions. In addition, the increments of magnetic field into the flow will increase value of skin friction coefficient and the heat transfer coefficient.

Keywords: *carbon nanotubes; boundary layer flow; moving plate; Haar wavelet; heat transfer; magneto-hydrodynamics.*

2010 MSC: 35Q35, 35Q79, 76A02, 76D05, 65D30 **DOI:** 10.23939/mmc2025.01.057

1. Introduction

The performance impact, energy efficiency, and operational costs of numerous processes are crucial for various industrial applications. Therefore, advancements in heat transfer technologies are essential. Traditionally, base fluids like water and kerosene have been used as heat transfer media. However, rising industrial demands for faster heat transfer have led to developed the innovative idea of mixing nanoparticles (NPs) with base fluids, resulting in the creation of nanofluids (NFs) Choi and Eastman [1]. Nanoparticles, which are particles with dimensions typically less than 100 nanometers, can significantly enhance the thermal properties of the base fluid. These nanoparticles can be made from a variety of materials, including metals (such as copper and aluminum), metal oxides (such as alumina and titania), and other advanced materials (such as carbon nanotubes and graphene).

Among various types of nanofluids, carbon nanotube (CNT) nanofluids are considered some of the most effective due to their exceptionally high thermal conductivity compared to other nanoparticles [2, 3]. Carbon nanotubes, which are cylindrical structures with nanoscale diameters and lengths that are categorized into single-walled carbon nanotubes (SWCNTs) and multi-walled carbon nanotubes (MWCNTs). CNTs are used in a wide range of applications such as biosensors for their high surface area and electrical conductivity, which improve the sensitivity and performance of these sensors [4–7],

This work was supported by Research Grant Putra, University Putra Malaysia.

various medical technologies, including drug delivery systems and imaging techniques, due to their biocompatibility and ability to interact with biological systems [8] and nanogenerator technologies, which convert mechanical energy into electrical energy [9]. CNTs exhibit a remarkable range of thermal conductivity values, from as low as 0.1 W/mK to as high as 6600 W/mK [10]. This broad spectrum of thermal conductivity is attributed to the structure, type of CNT, and the conditions under which they are measured.

Magneto-hydrodynamics (MHD) is a field that merges principles of both magnetism and fluid dynamics to study the behavior of electrically conductive fluids in the presence of a magnetic field [11]. Magnetic field typically increases the local skin friction coefficient because the Lorentz force acts as an additional body force in the fluid, enhancing the momentum transfer near the boundary layer and thus increasing friction. Experimental work by Masaaki et al. [12] demonstrated that the presence of a magnetic field enhances the heat transfer coefficient. This occurs because the magnetic field influences the thermal boundary layer, causing positive impact on energy transfer of heat from the fluid to the boundary. The interplay between magnetic forces and fluid dynamics opens up new avenues for optimizing systems where heat and mass transfer are critical.

Solving nonlinear ordinary differential equations (ODEs) over an infinite interval presents numerous difficulties, particularly when using numerical methods like the Shooting method and Finite element method, as well as semi-numerical methods such as perturbation parameters and Pade approximations. These methods often face limitations related to convergence, stability, and the need for accurate initial guesses when solving boundary value problems (BVPs). Due to these challenges, it is crucial to develop new efficient techniques that can overcome these obstacles and overall solving nonlinear ODEs over infinite intervals.

Wavelet methods have become increasingly prominent in numerical analysis due to their versatility and efficiency in handling various types of differential equations. This approach offers a compelling alternative to traditional numerical methods such as finite difference, finite element, and spectral methods. Key figures in the development of wavelet theory include Meyer, Morlet, Grossmann, and Daubechies [13], who made significant contributions to the mathematical underpinnings of wavelet functions. One of the earliest and most influential wavelet methods is the Haar wavelet, introduced by Alfred Haar in 1910. The Haar wavelet is particularly notable for its simplicity and consisting of step functions that are straightforward to manipulate. Due to its simple structure, the Haar wavelet requires fewer computations, making it suitable for real-time applications. Chen and Hsiao [14] developed operational matrices for Haar wavelets, that facilitate the transformation of differential equations into algebraic equations. Lepik [15] expanded on this work by creating a systematic and effective approach for solving differential equations on grids with uniform spacing. Karkera et al. [16] discussed the investigations of universal combined MHD flow of viscous boundary layer with Haar wavelets. By comparing their results with previously observed solutions, they have demonstrated that Haar wavelets provide a reliable and computationally efficient tool for analyzing complex fluid dynamics scenarios. Subsequent research has consistently demonstrated the accuracy and simplicity of Haar wavelets in solving boundary layer flow problems [17–20]. Based on published literature, this study examines the flow properties and heat transfer over a moving plate in the presence of carbon nanotubes and MHD effects.

2. Haar wavelets

The Haar wavelet is a square-shaped waves with a magnitude of ± 1 at certain intervals and zero elsewhere that forms a variety of wavelet families or basis. The Haar wavelet is classified as compact, dyadic, discrete, and orthonormal. It consists of pairs of piecewise constant functions and it is the numerically simplest of all wavelet families. The one-dimensional Haar wavelet family for $x \in [0, 1)$ can be defined as the Haar wavelet associated with the mother wavelet,

$$h_i(x) = \begin{cases} 1, & \text{for} \quad x \in [\alpha, \beta), \\ -1, & \text{for} \quad x \in [\beta, \gamma), \\ 0, & \text{elsewhere}, \end{cases}$$

where $\alpha = \frac{k}{m}$, $\beta = \frac{k+0.5}{m}$, $\gamma = \frac{k+1}{m}$. $h_1(x)$ is the scaling function for the family can be defined as

$$h_1(x) = \begin{cases} 1, & \text{for} \quad x \in [0,1), \\ 0, & \text{elsewhere.} \end{cases}$$

The Haar series is constructed by taking linear combinations of the scaled and translated Haar wavelet functions. These combinations are weighted by the coefficients depending on the properties original function. Haar wavelet integration also can be expanded into Haar series. One significant advantage of the Haar wavelet is the ability to integrate it analytically at arbitrary times. By referring to Karkera et al. [16], these integrals can be determined as follows:

$$p_{i,1}(t) = \int_0^x h_i(t)\,dt = \begin{cases} x-\alpha & \text{for} \quad x \in [\alpha,\beta), \\ \gamma - x & \text{for} \quad x \in [\beta,\gamma), \\ 0 & \text{elsewhere,} \end{cases}$$

$$p_{i,2}(t) = \int_0^x p_{i,1}(t)\,dt = \begin{cases} \frac{1}{2}(x-\alpha)^2 & \text{for} \quad x \in [\alpha,\beta), \\ \frac{1}{4m^2} - \frac{1}{2}(\gamma - x)^2 & \text{for} \quad x \in [\beta,\gamma), \\ \frac{1}{4m^2} & \text{for} \quad x \in [\gamma,1), \\ 0 & \text{elsewhere.} \end{cases}$$

Likewise,

$$P_{i,l+1}(t) = \int_0^t P_{i,l}(x')\,dx', \quad l = 2,3,\ldots.$$

3. Mathematical formulation

This model examines two-dimensional (2D) steady flow past a moving plate under the influence of a magnetic field. The flow is characterized as incompressible and laminar, involving SWCNTs and MWCNTs. Water and kerosene are chosen as the base fluids, following the findings of Yilmaz et al. [21], who noted that the choice of base fluids can significantly impact the heat transfer process. A Cartesian coordinate system is employed, with the x-axis parallel to the plate and the y-axis perpendicular to it. The plate is assumed to be kept at a uniform temperature T_w, while T_∞ denotes the temperature of the fluid far from the plate. The plate moves with a constant velocity U_w, and U_∞ represents the free stream velocity away from the plate's surface. The thermal properties of the carbon nanotubes and base fluids are provided in Tables 1 and 2.

Table 1. Thermophysical properties of CNTs and base fluids [22].

Physical properties	Nanoparticles		Base fluid	
	SWCNTs	MWCNTs	Water	Kerosene
ρ (kg/m^3)	2 600	1 600	997	783
C_p (J/kg K)	425	796	4 179	2 090
k (W/m K)	6 600	3 000	0.613	0.145

By extending and modifying the works from Bachok et al. [23] and Norzawary et al. [24], the boundary layer equations of continuity, momentum and energy for this model can be constructed as

$$\frac{\partial u}{\partial x} + \frac{\partial v}{\partial y} = 0, \tag{1}$$

$$u\frac{\partial u}{\partial x} + v\frac{\partial u}{\partial y} = \frac{\mu_{nf}}{\rho_{nf}}\frac{\partial^2 u}{\partial y^2} + \frac{\sigma_{nf}}{\rho_{nf}}B^2(U-u), \tag{2}$$

$$u\frac{\partial T}{\partial x} + v\frac{\partial T}{\partial y} = \alpha_{nf}\frac{\partial^2 T}{\partial y^2}. \tag{3}$$

along with the boundary conditions

$$\begin{aligned} u = U_w(x) = \lambda U, \quad v = V_w(x), \quad T = T_w \quad \text{at} \quad y = 0, \\ u \to U_\infty(x), \quad T \to T_\infty, \quad \text{as} \quad y \to \infty. \end{aligned} \tag{4}$$

The velocity components u and v represent the movement along the Cartesian coordinates (x, y), where the x-axis lies along the plate and the y-axis is perpendicular to it. The term μ_{nf}/ρ_{nf} can be simplified to $v_{nf} = \mu_{nf}/\rho_{nf}$, where v_{nf} denotes the effective kinematic viscosity. The uniform velocity of the free stream flow U is expressed as $U = U_w + U_\infty$. The temperature of the nanofluids is represented by T, and B denotes the magnetic field applied to the fluid flow. T_w is the constant temperature of the plate, while T_∞ is the temperature of the ambient fluid. In this context, λ and σ represent the velocity parameter and the Stefan–Boltzmann constant, respectively. The subscripts f, nf, and CNT refer to fluid, nanofluid, and carbon nanotube, respectively. The correlation of the physical properties is detailed in Table 2.

Table 2. Thermo-physical properties of CNTs Nanofluids [25].

Properties	CNTs nanofluids
Dynamic viscosity, μ_{nf}	$\mu_{nf} = \frac{\mu_f}{(1-\phi)^{(2.5)}}$
Density, ρ_{nf}	$\rho_{nf} = (1-\phi)\rho_f + \phi\rho_{CNT}$
Effective kinematic viscosity, v_{nf}	$v_{nf} = \frac{\mu_{nf}}{\rho_{nf}}$
Thermal conductivity, k_{nf}	$k_{nf} = k_f \frac{1-\phi+2\phi\frac{k_{CNT}}{k_{CNT}-k_f}\ln\frac{k_{CNT}+k_f}{2k_f}}{1-\phi+2\phi\frac{k_f}{k_{CNT}-k_f}\ln\frac{k_{CNT}+k_f}{2k_f}}$
Heat capacity, $(\rho C_p)_{nf}$	$(\rho C_p)_{nf} = (1-\phi)(\rho C_p)_f + \phi(\rho C_p)_{CNT}$
Thermal diffusivity, α_{nf}	$\alpha_{nf} = \frac{k_{nf}}{(\rho C_p)_{nf}}$

Using similarity transformation, the partial differential equations (PDEs) Eqs. (1)–(3) can be converted into ODEs. As a result, the independent variable changes to:

$$\eta = y\sqrt{\frac{U}{v_f x}}, \quad \psi = \sqrt{v_f x U}\, f(\eta), \quad \theta(\eta) = \frac{T - T_\infty}{T_w - T_\infty}, \tag{5}$$

where η is the independent variable and ψ represents the stream function, where $u = \frac{\partial\psi}{\partial y}$ and $v = -\frac{\partial\psi}{\partial x}$. By expressing the equations in a non-dimensional form, we simplify the number and complexity of variables, making it easier to define the governing equations of the investigated phenomena [26]. Using the similarity variables Eq. (1) is satisfied and the remaining Eqs. (2)–(3) are changed. From Eq. (5), we can transform the PDEs from Eqs. (2) and (3) into ODEs with respect to η as follows

$$\frac{1}{(1-\phi)^{(2.5)}\left(1-\phi+\frac{\phi\rho_{CNT}}{\rho_f}\right)} f''' + \frac{1}{2} f f'' + M(1-f') = 0, \tag{6}$$

$$\frac{1}{\Pr}\frac{k_{nf}/k_f}{1-\phi+\frac{\phi(\rho Cp)_{CNT}}{(\rho Cp)_f}}\theta'' + \frac{1}{2} f\theta' = 0. \tag{7}$$

Together with the boundary conditions

$$\begin{gathered} f(0) = 0, \quad f'(0) = \lambda, \quad \theta(0) = 1, \\ f'(\eta) \to (1-\lambda), \quad \theta(\eta) \to 0, \quad \text{as} \quad \eta \to \infty, \end{gathered} \tag{8}$$

where $M = \frac{\sigma_{nf} B_o^2}{\rho_{nf}\, 2U}$ is a magnetic fields parameter and λ is a moving parameter. In addition, Prandtl number is presented by $\Pr = \frac{v_f}{\alpha_f}$. Then, the physical quantities required are the coefficient of skin friction, C_f and sheer stress's surface, τ_w,

$$C_f = \frac{\tau_w}{\rho_f U^2}, \quad \tau_w = \mu_{nf}\left(\frac{\partial u}{\partial y}\right) \quad \text{at} \quad y = 0, \tag{9}$$

then the local Nusselt number, Nu_x and the heat flux's surface, q_w are

$$\mathrm{Nu}_x = \frac{x q_w}{k_f(T_w - T_\infty)}, \quad q_w = -k_{nf}\left(\frac{\partial T}{\partial y}\right) \quad \text{at} \quad y = 0. \tag{10}$$

Thus, the above physical quantities are

$$C_f\, \mathrm{Re}_x^{\frac{1}{2}} = \frac{1}{(1-\phi)^{(2.5)}} f''(0), \quad \mathrm{Nu}_x\, \mathrm{Re}_x^{-\frac{1}{2}} = -\left(\frac{k_{nf}}{k_f}\right)\theta'(0) \tag{11}$$

and $\mathrm{Re}_x = \frac{U_x}{v_f}$ is the local Reynold number.

Numerical solution by Haar wavelet collocation method (HWCM). The semi-infinite physical domain $[0,\infty)$ must be changed to suitable Haar wavelet context, where it can be reduced to $[0,1)$ by introducing the coordinate transformation $\xi = \frac{\eta}{\eta_\infty}$ and changing the variable to $F(\xi) = \frac{f(\eta)}{\eta_\infty}$ and $\theta_1(\xi) = \frac{\theta(\eta)}{\eta_\infty}$ to satisfy all the boundary conditions. Then, Eqs. (6) and (7) can be transformed to

$$\frac{1}{(1-\phi)^{(2.5)}\left(1-\phi+\frac{\phi\rho_{CNT}}{\rho_f}\right)}F'''(\xi)+\frac{1}{2}\eta_\infty^2 F(\xi)F''(\xi)+\eta_\infty^2 M(1-F'(\xi))=0, \tag{12}$$

$$\frac{1}{\Pr}\frac{k_{nf}/k_f}{1-\phi+\frac{\phi(\rho C_p)_{CNT}}{(\rho C_p)_f}}\theta_1''(\xi)+\frac{1}{2}\eta_\infty^2 F(\xi)\,\theta_1'(\xi)=0. \tag{13}$$

The boundary conditions of (8) are transformed to

$$\begin{gathered} F(0)=0,\quad F'(0)=\lambda,\quad F'(1)=1-\lambda,\quad \theta_1(0)=\frac{1}{n_\infty},\\ F'(\eta)\to(1-\lambda),\quad \theta_1(1)\to 0,\quad \text{as}\quad \eta\to\infty. \end{gathered} \tag{14}$$

The higher order of derivative for (12) and (13) are approximated by Haar wavelet,

$$F''(\xi)=\sum_{i=1}^{2^{J+1}} a_i h_i(\xi), \tag{15}$$

$$\theta_1''(\xi)=\sum_{i=1}^{2^{J+1}} d_i h_i(\xi). \tag{16}$$

The corresponding lower order of $F''(\xi)$, $F'(\xi)$, $F(\xi)$, $\theta_1'(\xi)$ and $\theta_1(\xi)$ are integrated using (15) and (16):

$$F''(\xi)=\sum_{i=1}^{2^{J+1}} a_i\left[p_{i,1}(\xi)-C_i\right]+1-2\lambda, \tag{17}$$

$$F'(\xi)=\sum_{i=1}^{2^{J+1}} a_i\left[p_{i,2}(\xi)-\xi C_i\right]+\xi\,(1-2\lambda)+\lambda, \tag{18}$$

$$F(\xi)=\sum_{i=1}^{2^{J+1}} a_i\left[p_{i,3}(\xi)-\frac{\xi^2}{2}C_i\right]+\frac{\xi^2}{2}\,(1-2\lambda)+\lambda\xi, \tag{19}$$

$$\theta_1'(\xi)=\sum_{i=1}^{2^{J+1}} d_i\left[p_{i,1}(\xi)-C_i\right]-\frac{1}{n_\infty}, \tag{20}$$

$$\theta_1(\xi)=\sum_{i=1}^{2^{J+1}} d_i\left[p_{i,2}(\xi)-\xi C_i\right]-\frac{\xi}{n_\infty}+\frac{1}{n_\infty}. \tag{21}$$

Then, the higher order Eqs. (12) and (13) together with Eqs. (17)–(21) by applying the collocation point,

$$\xi_1=\frac{1}{2^{J+1}}\left(l-\frac{1}{2}\right),\quad l=1,2,\ldots,2^{J+1}. \tag{22}$$

Hence, a numerical solution for the system of nonlinear equations with 2^{J+1} unknown wavelet coefficients can be derived.

4. Result and discussion

The analytical solutions for the ODEs in Eqs. (6) and (7), along with boundary condition Eq. (8) have been solved and the numerical solutions can be achieved using Maple software. The basic properties of nanoparticles and base fluid are shown in Table 3 [22].

Table 3. Thermophysical properties of CNTs and base fluids Khan et al. (2014) [22].

Physical Properties	Nanoparticles		Base fluid	
	SWCNTs	MWCNTs	Water	Kerosene
ρ (kg/m3)	2 600	1 600	997	783
C_p (J/kg K)	425	796	4 179	2 090
k (W/m K)	6 600	3 000	0.613	0.145

Figures 1 and 2 illustrate the impact of skin friction, $f''(0)$, and on the heat transfer coefficient, $-\theta'(0)$, in SWCNTs dispersion in water, considering the magnetic field, M, and the moving parameter, λ. With constants ϕ and Prandtl number Pr set at 0.1 and 6.2, respectively, and $M = 0$ indicating no magnetic influence, the plate's motion is either against ($\lambda < 0$) or with the free stream ($\lambda > 0$). The figures show unique solutions for $\lambda > 0$ and $M > 0.1$, and dual solutions for $\lambda_c \leqslant \lambda < 0$ and $M < 0.1$, with no solutions for $\lambda_c > \lambda$. The critical value λ_c determines whether dual solutions or no solutions occur. Increased M values enhance $f''(0)$ and $-\theta'(0)$, slowing thermal boundary layer separation, with the second solution showing a smaller increase in these values.

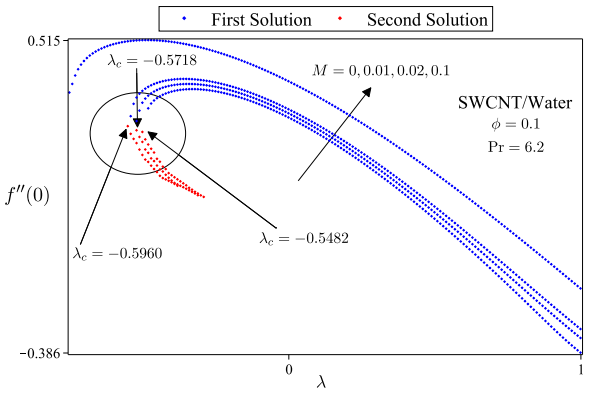

Fig. 1. Variation of $f''(0)$ with different M and λ for SWCNT/water.

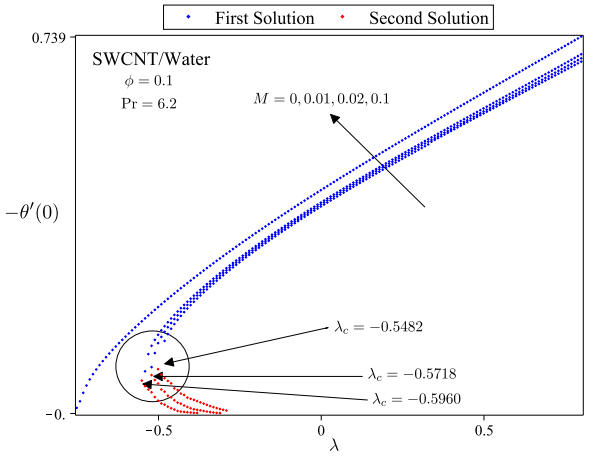

Fig. 2. Variation of $-\theta'(0)$ with different M and λ for SWCNT/water.

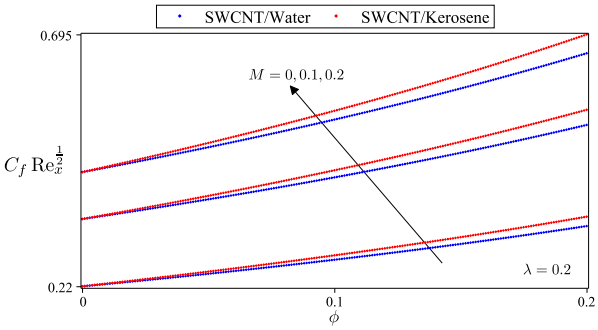

Fig. 3. Effect of different values of M on the skin friction coefficient using various ϕ for SWCNT/water and SWCNT/kerosene.

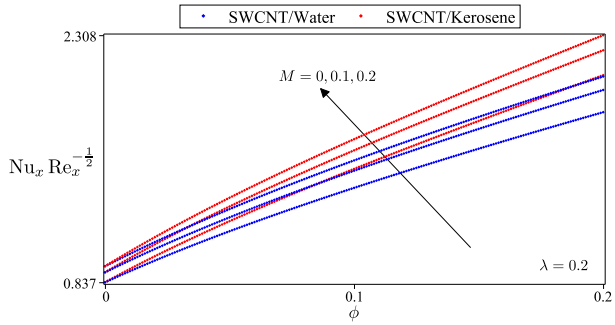

Fig. 4. Effect of different values of M on the Nusselt number using various ϕ for SWCNT/water and SWCNT/kerosene.

To determine which fluid is more effective, we examined the performance of SWCNT in water and kerosene across varying volume fractions, ϕ, from 0 to 0.2, as shown in Figures 3 and 4. These figures reveal that SWCNT in kerosene outperforms water in terms of skin friction and the local Nusselt number. Specifically, the graphs display changes in $C_f \, \mathrm{Re}_x^{\frac{1}{2}}$ and $\mathrm{Nu}_x \, \mathrm{Re}_x^{-\frac{1}{2}}$ for a moving parameter $\lambda = 0.2$. As ϕ increases, both $C_f \, \mathrm{Re}_x^{\frac{1}{2}}$ and $\mathrm{Nu}_x \, \mathrm{Re}_x^{-\frac{1}{2}}$ rise, particularly with higher values of M. This study highlights that SWCNT in kerosene performs better than in water, especially under increased M conditions.

Figures 5 and 6 compare the performance of SWCNT and MWCNT in water, with varying values of $M = 0, 0.1, 0.2$ and $0 \leqslant \phi \leqslant 0.2$. The graphs show that SWCNT consistently outperforms MWCNT in terms of the skin friction coefficient, $C_f \operatorname{Re}_x^{\frac{1}{2}}$, and the local Nusselt number, $\operatorname{Nu}_x \operatorname{Re}_x^{-\frac{1}{2}}$, for a constant moving parameter $\lambda = 0.2$. As M increases, both $C_f \operatorname{Re}_x^{\frac{1}{2}}$ and $\operatorname{Nu}_x \operatorname{Re}_x^{-\frac{1}{2}}$ also increase, demonstrating the significant impact of M and ϕ on the thermal and fluid dynamic properties of these nanotubes. Overall, the analysis highlights the superior efficiency of SWCNT over MWCNT in a water-based environment.

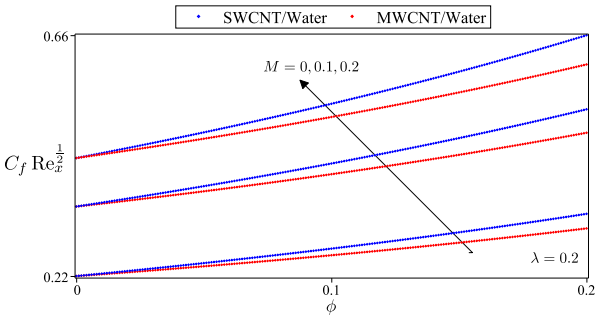

Fig. 5. Effect of different values of M on the skin friction coefficient using various ϕ for SWCNT/water and MWCNT/water.

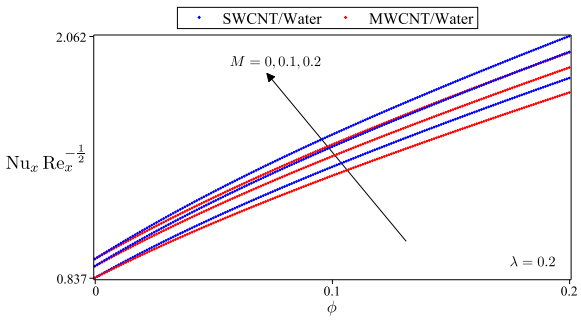

Fig. 6. Effect of different values of M on the Nusselt number using various ϕ for SWCNT/water and MWCNT/water.

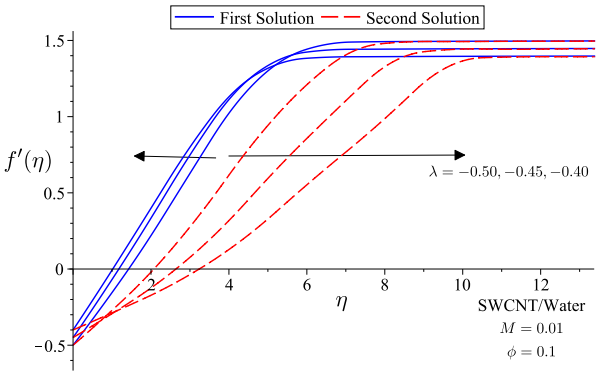

Fig. 7. Effect of different values of λ on the velocity profile using various η for SWCNT/water.

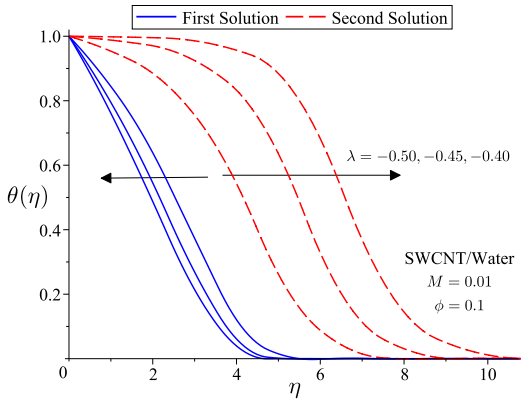

Fig. 8. Effect of different values of λ on the temperature profile using various η for SWCNT/water.

Figures 7 and 8 explore the velocity and temperature profiles of SWCNT dispersed in water, focusing on the impact of different values of the moving parameter, λ, on $f'(\eta)$ and $\theta(\eta)$. Here, the magnetic field parameter, $M = 0.01$, the volume fraction, $\phi = 0.1$, and $\lambda = -0.5, -0.45, -0.4$. These figures reveal noticeable differences in the thickness of the momentum and thermal boundary layers between the first and second solutions. Specifically, the second solution shows a larger boundary layer thickness compared to the first solution.

In the momentum boundary layer, the first solution shows an increase in the velocity profile, represented by $f'(\eta)$, while the second solution shows a decrease. This indicates contrasting flow patterns between the two solutions. Similarly, in the thermal boundary layer, the first solution shows a decrease in the temperature profile, $\theta(\eta)$, whereas the second solution shows an increase. This highlights the distinct thermal behavior of two solutions.

Figures 9 and 10 examine the velocity and temperature profiles of SWCNTs dispersed in water, focusing on the effects of varying magnetic field values $M = 0, 0.01, 0.02$ on $f'(\eta)$ and $\theta(\eta)$. Here, the parameter $\lambda = -0.45$, and the volume fraction, $\phi = 0.1$. The figures reveal a clear difference in the thickness of the momentum and thermal boundary layers between the two solutions, with the second solution showing thicker boundary layers than the first.

In the momentum boundary layer, the velocity profile $f'(\eta)$ increases for the first solution but decreases for the second, indicating different flow characteristics. Similarly, in the thermal boundary layer, the temperature profile $\theta(\eta)$ decreases for the first solution but increases for the second, highlighting distinct thermal behaviors between the two solutions.

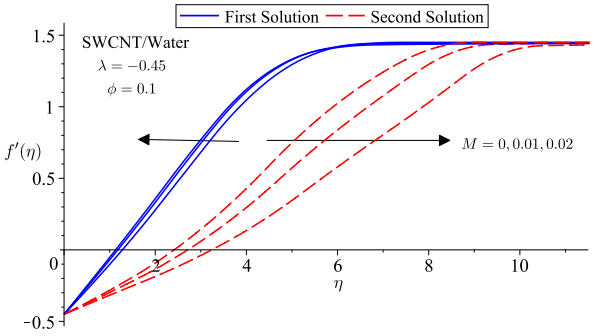

Fig. 9. Effect of different values of M on the temperature profile using various η for SWCNT/water.

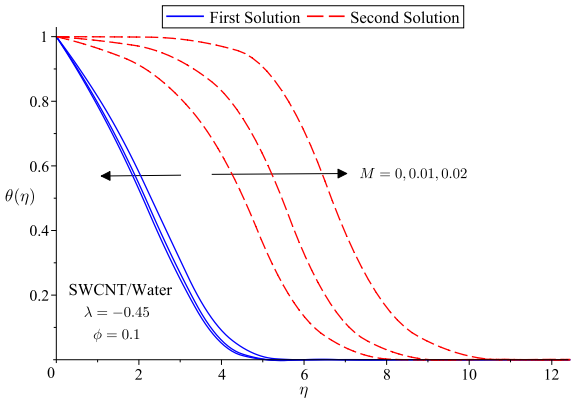

Fig. 10. Effect of different values of M on the temperature profile using various η for SWCNT/water.

5. Conclusion

The problem of flow and heat transfer over a moving plate in a carbon nanotubes with MHD effect was studied numerically. The consideration of the parameters such as volume fractions ϕ, moving parameter λ and magnetic parameter M were solved using numerical technique based on Haar wavelets collocation in Maple software.

- For moving surface, the solutions are unique when the moving parameter $\lambda > 0$, represents that the plate moves in the same direction as the free stream while the duality solution exist, when $\lambda_c \leqslant \lambda < 0$, represents the plate moves in opposite direction as the free stream.
- The increment value of magnetic parameter in carbon nanotubes can increases the skin friction coefficient and heat transfer coefficient. The range of dual solutions widen as the value M increases.
- Skin friction coefficient and heat transfer coefficient performs better in kerosene-based CNTs compared to water-based CNTs.
- SWCNTs with higher density unlike MWCNTs cause it to be more effectual in skin friction coefficient and heat transfer coefficient rate.

[1] Choi S. U. S, Eastman J. A. Enhancing thermal conductivity of fluids with nanoparticles. Argonne National Lab. (ANL), Argonne, IL (United States), (1995).

[2] Ali N., Bahman A. M., Aljuwayhel N. F., Ebrahim S. A., Mukherjee S., Alsayegh A. Carbon-based nanofluids and their advances towards heat transfer applications — A review. Nanomaterials. **11** (6), 1628 (2021).

[3] Lee D.-K., Yoo J., Kim H., Kang B.-H., Park S.-H. Electrical and thermal properties of carbon nanotube polymer composites with various aspect ratios. Materials. **15** (4), 1356 (2022).

[4] Zhang C., Du X. Electrochemical sensors based on carbon nanomaterial used in diagnosing metabolic disease. Frontiers in Chemistry. **8**, 651 (2020).

[5] Bruzaca E. E. S., de Oliveira R. C., Duarte M. S. S., Sousa C. P., Morais S., Correia A. N., de Lima-Neto P. Electrochemical sensor based on multi-walled carbon nanotubes for imidacloprid determination. Analytical Methods. **13** (18), 2124–2136 (2021).

[6] Cho G., Azzouzi S., Zucchi G., Lebental B. Electrical and electrochemical sensors based on carbon nanotubes for the monitoring of chemicals in water — A review. Sensors. **22** (1), 218 (2022).

[7] Norizan M. N., Moklis M. H., Demon S. Z. N., Halim N. A., Samsuri A., Mohamad I. S., Knight V. F., Abdullah N. Carbon nanotubes: functionalisation and their application in chemical sensors. RSC Advances. **10** (71), 43704–43732 (2020).

[8] Zhang C., Wu L., de Perrot M., Zhao X. Carbon nanotubes: A summary of beneficial and dangerous aspects of an increasingly popular group of nanomaterials. Frontiers in Oncology. **11**, 693814 (2021).

[9] Afsarimanesh N., Nag A., Md. Eshrat e Alahi, Sarkar S., Mukhopadhyay S., Sabet G. S., Altinsoy M. E. A critical review of the recent progress on carbon nanotubes-based nanogenerators. Sensors and Actuators A: Physical. **344**, 113743 (2022).

[10] Kumanek B., Janas D. Thermal conductivity of carbon nanotube networks: A review. Journal of Materials Science. **54** (10), 7397–7427 (2019).

[11] Arulmozhi S., Sukkiramathi K., Santra S. S., Edwan R., Fernandez-Gamiz U., Noeiaghdam S. Heat and mass transfer analysis of radiative and chemical reactive effects on MHD nanofluid over an infinite moving vertical plate. Results in Engineering. **14**, 100394 (2022).

[12] Motozawa M., Chang J., Sawada T., Kawaguchi Y. Effect of magnetic field on heat transfer in rectangular duct flow of a magnetic fluid. Physics Procedia. **9**, 190–193 (2010).

[13] Daubechies I. Ten Lectures on Wavelets. CBMS-NSF Regional Conference Series in Applied Mathematics (1992).

[14] Chen C. F., Hsiao C. H. Haar wavelet method for solving lumped and distributed-parameter systems. IEE Proceedings-Control Theory and Applications. **144** (1), 87–94 (1997).

[15] Lepik Ü. Numerical solution of differential equations using Haar wavelets. Mathematics and Computers in Simulation. **68** (2), 127–143 (2005).

[16] Karkera H., Katagi N. N., Kudenatti R. B. Analysis of general unified MHD boundary-layer flow of a viscous fluid – a novel numerical approach through wavelets. Mathematics and Computers in Simulation. **168**, 135–154 (2020).

[17] Awati V. B., Kumar M., Wakif A. Haar wavelet scrutinization of heat and mass transfer features during the convective boundary layer flow of a nanofluid moving over a nonlinearly stretching sheet. Partial Differential Equations in Applied Mathematics. **4**, 100192 (2021).

[18] Safian N. A. A., Rasedee A. F. N., Bachok N., Mahad Z., Hasan M. Haar wavelet collocation method for solving stagnation point flow over a nonlinearly stretching/shrinking sheet in a carbon nanotube with slip effect. Mathematical Modeling and Computing. **10** (4), 1281–1291 (2023).

[19] Hasanah N. S., Rasedee A. F. N., Bachok N., Wong T. J., Hasan M. Haar wavelet collocation method for solving stagnation point over a nonlinearly stretching/shrinking sheet in a hybrid nanofluid with slip effect. Mathematical Modeling and Computing. **10** (4), 1269–1280 (2023).

[20] Awati V. B., Goravar A., Kumar M. Spectral and Haar wavelet collocation method for the solution of heat generation and viscous dissipation in micro-polar nanofluid for MHD stagnation point flow. Mathematics and Computers in Simulation. **215**, 158–183 (2024).

[21] Duygu Y. A., Gürü M., Sözen A., Çiftçi E. Investigation of the effects of base fluid type of the nanofluid on heat pipe performance. Proceedings of the Institution of Mechanical Engineers, Part A: Journal of Power and Energy. **235** (1), 124–138 (2021).

[22] Khan W. A., Khan Z. H., Rahi M. Fluid flow and heat transfer of carbon nanotubes along a flat plate with Navier slip boundary. Applied Nanoscience. **4**, 633–641 (2014).

[23] Bachok N., Ishak A., Pop I. Boundary-layer flow of nanofluids over a moving surface in a flowing fluid. International Journal of Thermal Sciences. **49** (9), 1663–1668 (2010).

[24] Norzawary N. H. A., Bachok N., Ali F. M. Boundary Layer Flow and Heat Transfer on A Moving Plate in A Carbon Nanotubes. Journal of Multidisciplinary Engineering Science and Technology. **6** (12), 62–67 (2019).

[25] Samat N. A. A., Bachok N., Arifin N. M. Carbon Nanotubes (CNTs) Nanofluids Flow and Heat Transfer under MHD Effect over a Moving Surface. Journal of Advanced Research in Fluid Mechanics and Thermal Sciences. **103** (1), 165–178 (2023).

[26] Conejo A. N. Fundamentals of Dimensional Analysis. Theory and Applications in Metallurgy. Springer Nature (2021).

Метод колокації вейвлетів Хаара для розв'язання задачі потоку та теплообміну прикордонного шару над рухомою пластиною у вуглецевих нанотрубках з МГД-ефектом

Хасваніза Н. С.[1], Раседі А. Ф. Н.[2], Бачок Н.[1], Хасан М.[4]

[1] *Кафедра математики та статистики, Факультет природничих наук, Університет Путра Малайзії, 43400 Серданг, Селангор, Малайзія*
[2] *Факультет економіки та Муамалат, Університет Саінс Ісламм Малайзії, Малайзія*
[3] *Кафедра фундаментальних наук та техніки, Факультет сільського господарства та харчових наук, Університет Путра Малайзія, Кампус Бінтулу, Ньябау Роуд, Бінтулу, Саравак, 97008, Малайзія*
[4] *Центр фундаментальних досліджень у галузі науки Університету Путра Малайзії*

Метою цього дослідження є розгляд потоку прикордонного шару та теплопередачі над рухомою пластиною з наявністю магнітогідродинаміки на поверхні вуглецевих нанотрубок. Отримано та розв'язано математичну модель для задачі течії в прикордонному шарі за допомогою чисельних методів на основі колокації вейвлетів Хаара. У цій статті використовувалися такі типи наночастинок: одностінні та багатошарові вуглецеві нанотрубки з водою та гасом, які використовувалися як базова рідина. Диференціальні рівняння в частинних похідних перетворюються на нелінійні звичайні диференціальні рівняння шляхом перетворення подібності. Для роботи з цими рівняннями використовується програмне забезпечення Maple. Результати були представлені у вигляді графіків, що включають профіль швидкості та температури, коефіцієнт поверхневого тертя та локальне число Нуссельта для різних значень магнітного поля, об'ємного тертя CNT та параметра переміщення. Отримані результати полягають у тому, що рухома пластина дає не єдиний розв'язок. Крім того, прирости магнітного поля в потоці призведуть до збільшення значення коефіцієнта поверхневого тертя і коефіцієнта теплообміну.

Ключові слова: *вуглецеві нанотрубки; течія прикордонного шару; рухома пластина; вейвлет Хаара; теплообмін; магнітогідродинаміка.*